Wave Inversion Technology, Report No. 4, pages 75-86

Offset-dependent resolution of seismic migration

J. Schleicher and L.T. Santos[1]

keywords: *resolution, seismic migration, Fresnel zone*

ABSTRACT

In this work, we study the resolving power of seismic migration as a function of source-receiver offset. We quantify horizontal resolution by means of the region around the migrated reflection point that is influenced by the migrated elementary wave. To obtain an estimate for the mentioned zone of horizontal influence *after migration, we investigate the migration output at a chosen depth point in the vicinity of the specular reflection point, i.e., when the output point is moved along the reflector. We find that the region of influence is well approximated by the difference between the time-domain Fresnel zone and its paraxial approximation. The width of the spatial resolution resulting from migration of the reflection event is compared with the resolution predicted from theoretical ray-theory formulas for various data sets with different offsets. It is to be remarked that the above resolution is reached only with perfect, noise-free, correctly sampled, unbiased data.*

INTRODUCTION

Seismic resolution after depth migration has been theoretically discussed by various authors (Berkhout, 1984; Beylkin, 1985; Cohen et al., 1986; Bleistein, 1987). A recent comprehensive study on the subject was carried out in Vermeer (1999), where additional references on the subject can be found.

It is widely accepted among geophysicists that 'depth migration reduces the Fresnel zone'. Although this is a very sloppy expression, because the Fresnel zone is a fixed-size frequency-dependent quantity associated with the reflected ray, we will see in this section that there is a lot of truth in it.

We discuss horizontal resolution in a completely analogous manner to the discussion of the pulse stretch in Tygel et al. (1994) that is closely related to vertical resolution. Note that we implicitly define now resolution in a slightly different way from what is usually done in the literature. Conventionally, resolution is quantified

[1]**email:** js@ime.unicamp.br

by the minimal distance of two objects such that their images can still be recognized as two distinct ones. In this way, resolution is clearly a frequency-domain concept. For a more practical, time-domain concept, we need a different definition. Guided by the above section on pulse distortion, we quantify horizontal resolution by means of the region around the migrated reflection point M_R that is influenced by the migrated elementary wave at M_R.

To obtain an estimate for the mentioned zone of 'horizontal influence' after migration, we investigate the migration output at the chosen depth point $M = \overline{M}_R$ in the vicinity of the specular reflection point M_R (see Figure 1), i.e., when the output point is moved along the reflector Σ_R.

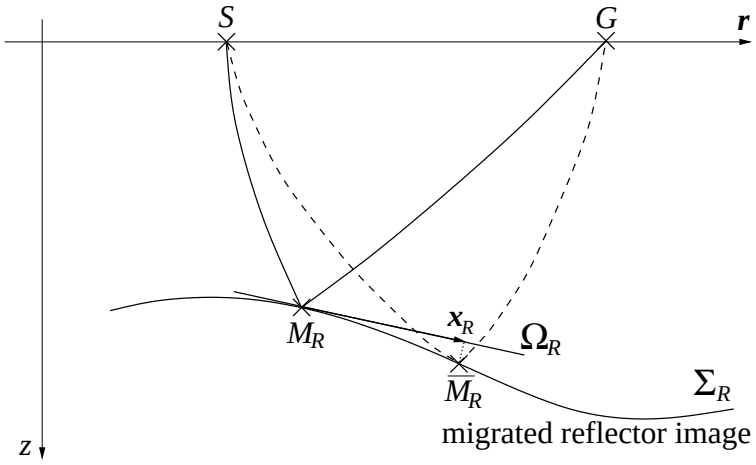

Figure 1: Horizontal resolution: influence of the migrated event at the specular reflection point M_R on the migration result at the neighboring point $\overline{M}_R$ on the reflector.

In particular, we study the horizontal resolution of seismic migration as a function of offset. As shown by Tygel et al. (1994), the vertical resolution is the worse the greater the offset becomes. For a horizontal reflector below a constant-velocity overburden, it decreases proportionally to the cosine of the reflection angle. A similiar behaviour is expected for horizontal resolution.

MATHEMATICAL DERIVATION

As the starting point, we consider the time-dependent diffraction-stack integral in the form of Tygel et al. (1994),

$$V(M,t) \;=\; \frac{-1}{2\pi} \iint\limits_{A} d^2\vec{\xi}\, B(\vec{\xi}, M)\; \dot{F}[t + \mathcal{T}_{\text{dif}}(\vec{\xi}, M)], \tag{1}$$

where A denotes the migration aperture, B includes all amplitude factors being the weight function and the seismic data amplitude, and $\mathcal{T}_{\text{dif}}(\vec{\xi}, M)$ is the difference between the stacking surface, i.e., the diffraction traveltime $\mathcal{T}_D(\vec{\xi}, M)$, and the reflection traveltime $\mathcal{T}_R(\vec{\xi})$. The searched-for diffraction-stack migration result at M is given by the imaging condition $t = 0$, $V(M) = V(M, 0)$.

Applying the Fourier transform with respect to t to equation (1), we obtain according to familiar rules,

$$\hat{V}(M, \omega) \;=\; \hat{F}[\omega] \; \frac{i\omega}{2\pi} \iint\limits_{A} d^2\vec{\xi} \, B(\vec{\xi}, M) \; e^{i\omega \mathcal{T}_{\text{dif}}(\vec{\xi}, M)} \; . \tag{2}$$

We consider a Taylor-series expansion of $\hat{V}(\overline{M}_R, \omega)$ in $\vec{x}_R$ in the plane Ω_R tangent to the reflector at M_R (see Figure1). Due to Fermat's principle, we will need a second-order series

$$\hat{V}(\overline{M}_R, \omega) = \hat{V}(M_R, \omega) + \vec{\nabla}_R \hat{V}(M_R, \omega)\vec{x}_R + \frac{1}{2}\vec{x}_R \cdot \boldsymbol{V}_R(M_R, \omega)\vec{x}_R \, , \tag{3}$$

where $\vec{\nabla}_R \hat{V}$ is the gradient and $\boldsymbol{V}_R$ is the second-order derivative (Hessian) matrix of $\hat{V}(\overline{M}_R, \omega)$ with respect to x_{R1} and x_{R2} taken at M_R.

The stack result, $\hat{V}(M_R, \omega)$ is given, after asymptotic evaluation of this integral upon the use of the Method of Stationary Phase (Bleistein, 1984), by

$$\hat{V}(M_R, \omega) \;\simeq\; \hat{F}[\omega] \; \Upsilon(\vec{\xi}^*; M_R) \; , \tag{4}$$

where the new amplitude $\Upsilon(\vec{\xi}^*; M_R)$ includes the amplitude factor B of integral (1) together with some additional factors that appear as a consequence of the stationary-phase analysis. Moreover, $\vec{\xi}^*$ denotes the stationary or critical point, i.e., the point that satisfies the following stationarity condition

$$\vec{\nabla}_\xi \mathcal{T}_{\text{dif}}(\vec{\xi}, M)\Big|_{\vec{\xi} = \vec{\xi}^*} = \vec{0} \; . \tag{5}$$

Here, we assume that one and only one critical point $\vec{\xi}^*$ exists in the aperture range A which satisfies equation (5). If no critical point $\vec{\xi}^*$ exists in A, the diffraction-stack output will be asymptotically small. On the other hand, if more than one critical point exists in A, the stack result will be a sum of the contributions from each single one. These contributions will show, in general, different amplitudes and different distortions. Therefore, the migrated pulse is no longer under control. However, for most of the usual seismic measurement configurations (e.g., common shot or constant offset), the latter situation is extremely unlikely, as this means that a second ray connecting the same source-receiver pair would reflect at the same depth point.

The derivations of $\hat{V}(\overline{M}_R, \omega)$ with respect to the components of $\vec{x}_R$ are given by

$$\frac{\partial \hat{V}}{\partial x_{Rj}}(\overline{M}_R, \omega) = \hat{F}[\omega]\frac{i\omega}{2\pi}\iint\limits_A \left(i\omega \frac{\partial \mathcal{T}_{\text{dif}}}{\partial x_{Rj}} B + \frac{\partial B}{\partial x_{Rj}} \right) e^{i\omega \mathcal{T}_{\text{dif}}(\vec{\xi}, M)} \,. \tag{6}$$

Since $\mathcal{T}_R$ is not a function of $\vec{x}_R$, we observe that

$$\frac{\partial \mathcal{T}_{\text{dif}}}{\partial x_{Rj}} = \frac{\partial \mathcal{T}_D}{\partial x_{Rj}} = \frac{\partial \mathcal{T}_\Sigma}{\partial x_{Rj}} \,, \tag{7}$$

where we have used the notation $\mathcal{T}_\Sigma$ for the diffraction-traveltime function along rays connecting an arbitrary source-receiver pair defined by $\vec{\xi}$ to an arbitrary point on the reflector Σ. Fermat's principle states then that

$$\left.\frac{\partial \mathcal{T}_\Sigma}{\partial x_k}\right|_{\vec{x}=\vec{x}_R} = 0 \,. \tag{8}$$

Differentiating equation (6) a second time yields

$$\begin{aligned} \frac{\partial^2 \hat{V}}{\partial x_{Rj} \partial x_{Rk}}(\overline{M}_R, \omega) \;=\; & \hat{F}[\omega]\frac{i\omega}{2\pi}\iint\limits_A \left[i\omega \frac{\partial^2 \mathcal{T}_\Sigma}{\partial x_{Rj}\partial x_{Rk}} B + i\omega \frac{\partial \mathcal{T}_\Sigma}{\partial x_{Rj}} \frac{\partial B}{\partial x_{Rk}} + \right. \\ & \left. + (i\omega)^2 \frac{\partial \mathcal{T}_\Sigma}{\partial x_{Rj}} \frac{\partial \mathcal{T}_\Sigma}{\partial x_{Rk}} B + \frac{\partial^2 B}{\partial x_{Rj}\partial x_{Rk}} + i\omega \frac{\partial \mathcal{T}_\Sigma}{\partial x_{Rk}} \frac{\partial B}{\partial x_{Rj}} \right] e^{i\omega \mathcal{T}_{\text{dif}}(\vec{\xi}, M)} \,, \end{aligned} \tag{9}$$

where we have again used equation (7).

In high-frequency approximation, equations (6) and (9) are dominated by the highest-order non-vanishing terms in ω. At M_R, the first derivative of $\mathcal{T}_\Sigma$ vanishes due to Fermat's principle, equation (8). Thus, we find in this approximation,

$$\frac{\partial \hat{V}}{\partial x_{Rj}}(M_R, \omega) = 0 \tag{10}$$

and

$$\frac{\partial^2 \hat{V}}{\partial x_{Rj}\partial x_{Rk}}(M_R, \omega) = \hat{F}[\omega]\frac{(i\omega)^2}{2\pi}\iint\limits_A \frac{\partial^2 \mathcal{T}_\Sigma}{\partial x_{Rj}\partial x_{Rk}} B(\vec{\xi}, M_R) e^{i\omega \mathcal{T}_{\text{dif}}(\vec{\xi}, M_R)} \,. \tag{11}$$

The asymptotic evaluation of equation (11) is completely parallel to that of integral (2) and yields

$$\frac{\partial^2 \hat{V}}{\partial x_{Rj}\partial x_{Rk}} = \frac{\partial^2 \mathcal{T}_\Sigma}{\partial x_{Rj}\partial x_{Rk}} i\omega \hat{F}[\omega] \Upsilon(\vec{\xi}, M_R) \tag{12}$$

Here, we recognize the Hessian matrix $\boldsymbol{H}_F$ as defined by Hubral et al. (1992). We thus write in matrix form,

$$\boldsymbol{V}_R = \boldsymbol{H}_F i\omega \hat{F}[\omega] \Upsilon(\vec{\xi}, M_R) \,. \tag{13}$$

We now substitute equations (4), (10) and (12) in the Taylor series (3) to obtain

$$\hat{V}(\overline{M}_R,\omega) = \left[1 + i\omega\frac{1}{2}\vec{x}_R \cdot \boldsymbol{H}_F\vec{x}_R\right]\hat{F}[\omega]\Upsilon(\vec{\xi},M_R)\,. \tag{14}$$

Back in the time domain, this reads

$$V(\overline{M}_R,t) = \left[F[t] + \frac{1}{2}\vec{x}_R \cdot \boldsymbol{H}_F\vec{x}_R\dot{F}[t]\right]\Upsilon(\vec{\xi},M_R)\,, \tag{15}$$

or, at $t = 0$,

$$V(\overline{M}_R) = V(\overline{M}_R,0) = \left[F[0] + \frac{1}{2}\vec{x}_R \cdot \boldsymbol{H}_F\vec{x}_R\dot{F}[0]\right]\Upsilon(\vec{\xi},M_R)\,. \tag{16}$$

This result can again be interpreted as a first-order Taylor expansion of

$$V(\overline{M}_R) = F[\frac{1}{2}\vec{x}_R \cdot \boldsymbol{H}_F\vec{x}_R]\Upsilon(\vec{\xi},M_R)\,. \tag{17}$$

The physical interpretation of this result is straightforward. Since $F[t]$ is zero outside the interval $0 \le t \le \mathcal{T}_\varepsilon$, the influence of the migrated wavefield at M_R ends at that particular point $\overline{M}_R$, where

$$\frac{1}{2}\vec{x}_R \cdot \boldsymbol{H}_F\vec{x}_R = \mathcal{T}_\varepsilon\,. \tag{18}$$

This is exactly the definition of the time-domain Fresnel zone (Hubral et al., 1992). Thus, the area affecting the reflected field in the vicinity of M_R is the area of the paraxial Fresnel zone at M_R.

Let us appreciate the meaning of this result. We know that forward wave propagation distributes the information scattered from each "diffraction point" M in the seismic data over one projected Fresnel zone, which is therefore the minimum aperture for seismic Kirchhoff prestack depth migration (Schleicher et al., 1997). The present result tells us that migration smears the information pertaining to each depth point is smeared in the migrated section over a paraxial Fresnel zone. To undo the effects of wave propagation, that is, to recover the migrated image with a perfect resolution, however, it should smear this information over the true time-domain Fresnel zone. Thus, we can expect that the migrated data will show a lateral resolution that is roughly equivalent to the quality of the paraxial approximation of the Fresnel zone. In the next section, we confirm this conclusion with a simple numerical experiment.

SYNTHETIC EXAMPLE

To demonstrate the lateral resolution of seismic Kirchhoff depth migration, we have devised the following simple numerical experiment. Consider a horizontal interface

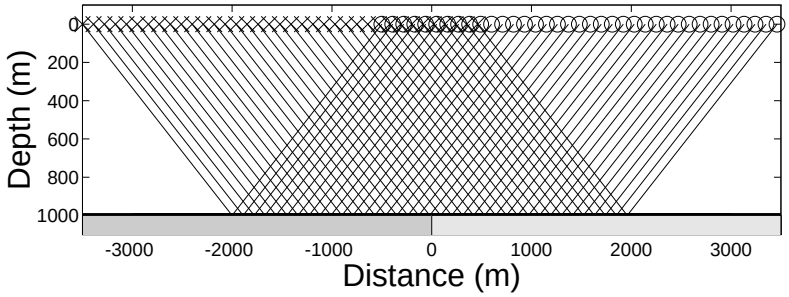

Figure 2: Earth model for a simple numerical experiment. Also shown is the ray family for a common-offset experiment with a source-receiver offset of 3000 m.

below a homogeneous halfspace with an acoustic wave velocity of 6 km/s (see Figure 2). Below the interface, we consider a vertical fault at $x = 0$ km, separating two homogeneous blocks with velocities of 5 km/s and 5.5 km/s on the left and right side of the fault, respectively. In this model, we have simulated an ensemble of common-offset seismic surveys with source-receiver offsets ranging from 0 m to 4000 m. The reflection angle for the largest offset is about 68°. A typical common-offset dataset (for a source-receiver offset of 3000 m) is depicted in Figure 3. The numerical model-

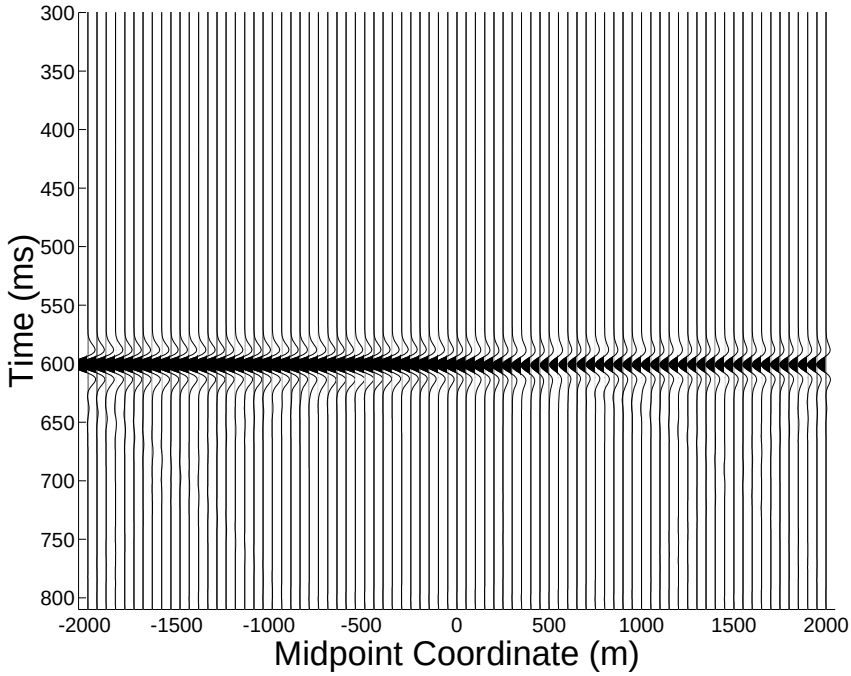

Figure 3: A numerically simulated common-offset dataset for the model in Figure 2.

ing was realized by an implementation of the 2.5-dimensional Kirchhoff integral. The source wavelet is a symmetrical Ricker wavelet with a duration of 64 ms.

The model was chosen to demonstrate the capacity of Kirchhoff migration to collapse the Fresnel zone. The simple fault model is ideal for this demonstration as it allows for a quantitative estimate of the residual Fresnel zone after migration. The Kirchhoff data show how the information of the fault is distributed in the seismic amplitudes over a projected Fresnel zone. To make this even more evident, we have picked the peak amplitude along the seismic event in Figure 3. This amplitude is shown in Figure 4 as a function of midpoint coordinate. Also indicated in Figure 4 are

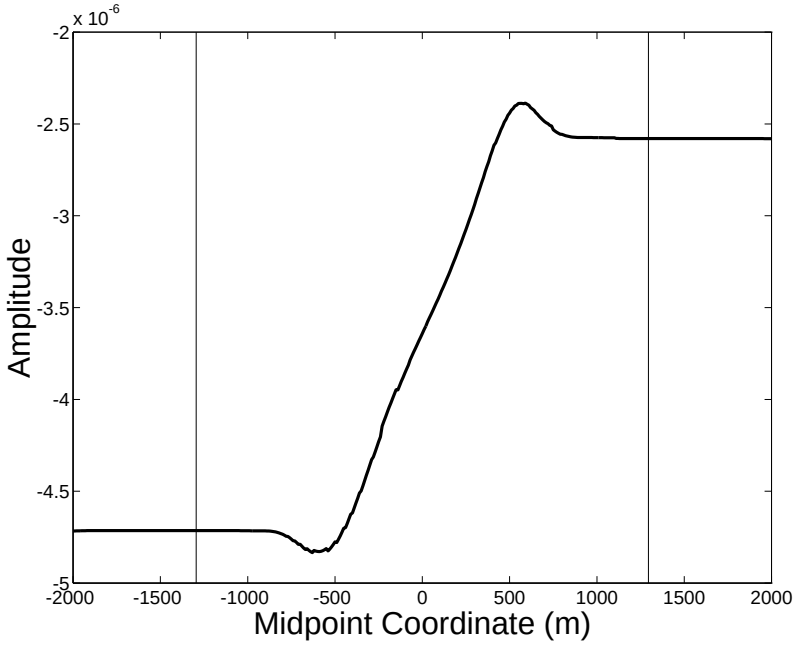

Figure 4: Seismic peak amplitude along the reflection event in Figure 3. Also indicated are the boundaries of the time-domain projected Fresnel zone in the direction of the seismic line.

the boundaries of the time-domain projected Fresnel zone. For a common-offset experiment over a model with a horizontal reflector below an overburden with a constant velocity v, the projected Fresnel zone is an ellipse with semi-axes

$$b = \sqrt{v\mathcal{T}_\varepsilon z}\ , \qquad a = \frac{b}{\cos^{3/2}\alpha}\ , \tag{19}$$

where $\mathcal{T}_\varepsilon$ is the length of the source wavelet, z is the reflector depth and α is the reflection angle. Indicated in Figure 4 is the size of the greater semi-axis a that quantifies the extension of the Fresnel zone in the direction of the seismic line. We observe that the abrupt horizontal velocity contrast leads to a smooth amplitude increase along the seismic reflection event, almost covering a complete projected Fresnel zone.

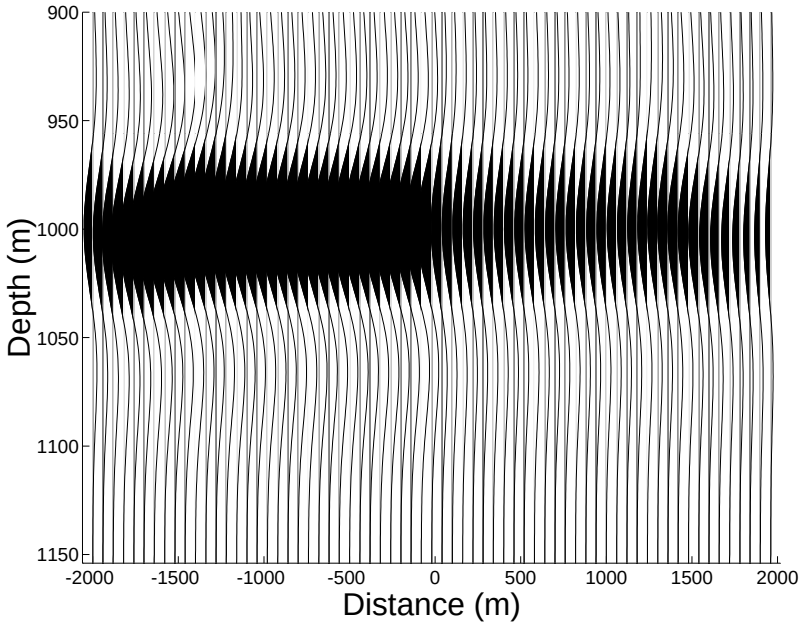

Figure 5: Depth section after a true-amplitude Kirchhoff migration of the data in Figure 3.

Figure 5 shows the data of Figure 3 after application of a seismic prestack Kirchhoff depth migration. The same prestack depth migration has been performed on all other corresponding synthetic common-offset sections with source-receiver offsets between 0 m and 4000 m. The results of these migrations are similar to that of Figure 5 and are, thus, not depicted here. We already recognize in Figure 5 that the amplitude change from one side of the fault to the other has become much steeper than in the original data (cf. Figure 3). This comes as no surprise since it is well-known that migration increases the lateral resolution. To better quantify this effect, Figure 6 shows the picked peak amplitudes along the seismic event in Figure 5. In this figure, it is much easier to observe than in Figure 5 that the change in amplitudes between the two values of the reflection coefficient at both sides of the fault is much more abrupt than in Figure 4. The Fresnel zone has indeed been strongly reduced by Kirchhoff migration. Our theoretical estimate for the size of the residual Fresnel zone after migration, based on the results of the previous section, is indicated by two vertical bars. These show the extension of the difference between the true time-domain Fresnel zone and its paraxial approximation. We see that this estimate provides a pretty good estimate of the actual size of the residual Fresnel zone.

To put this investigation on a broader basis and make its results more conclusive, we have repeated this numerical comparison for the other source-receiver offsets between 0 m and 4000 m. Figure 7 shows the size of the residual Fresnel zone after mi-

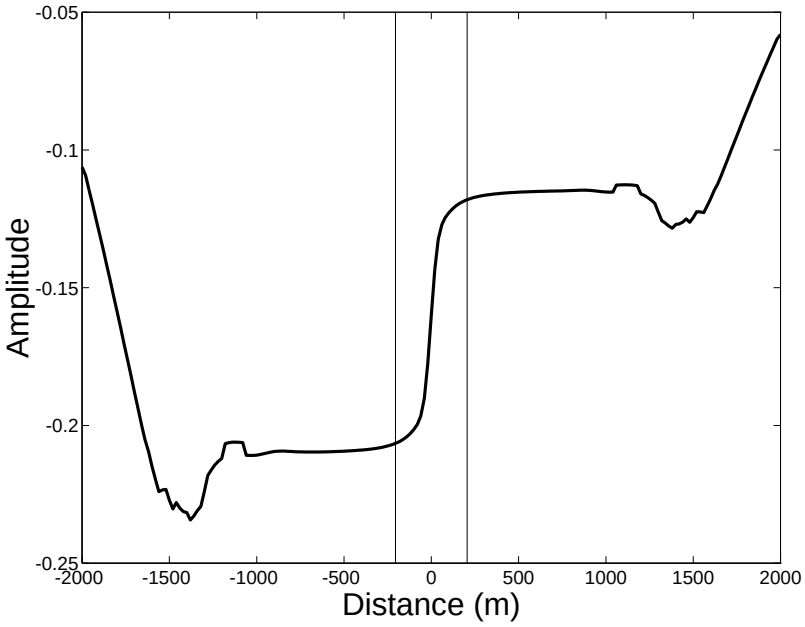

Figure 6: Picked peak amplitudes of the migrated reflection event in Figure 5.

gration as a function of offset (open circles). The size of the residual Fresnel zone after migration was estimated by determining where the amplitude values in the transition zone reach the value of the reflection coefficient as recovered by the true-amplitude migration. Because of the numerical error, this cannot be used as an exact criterion. We therefore chose the value of the recovered reflection coefficient to be reached where the error was less than six percent. Figure 7 compares the size of the residual Fresnel zone as estimated in this way to its predicted size (solid line) as calculated by the difference of the paraxial and true time-domain Fresnel zones. We observe quite a good agreement of estimated and predicted values over the whole range of offsets.

Note that the above results explain a well-known practical observation. It has been frequently observed in practice that zero- and near-offset data can provide a better lateral resolution than far-offset data. With the above considerations in mind, we now understand this fact. The reason is that the paraxial approximation to the Fresnel zone is the worse the farther the offsets are.

By means of the present analysis, we have now gained a much more quantitative understanding of what the common expression “depth migration reduces the Fresnel zone” means in quantitative terms. Speaking implicitly in time-domain concepts, the zone of influence reduces from the projected Fresnel zone described by the Hessian matrix $\boldsymbol{H}_P$ to the difference between the paraxial Fresnel zone described by matrix $\boldsymbol{H}_F$ and the true Fresnel zone. It is to be remarked, however, that the above resolution

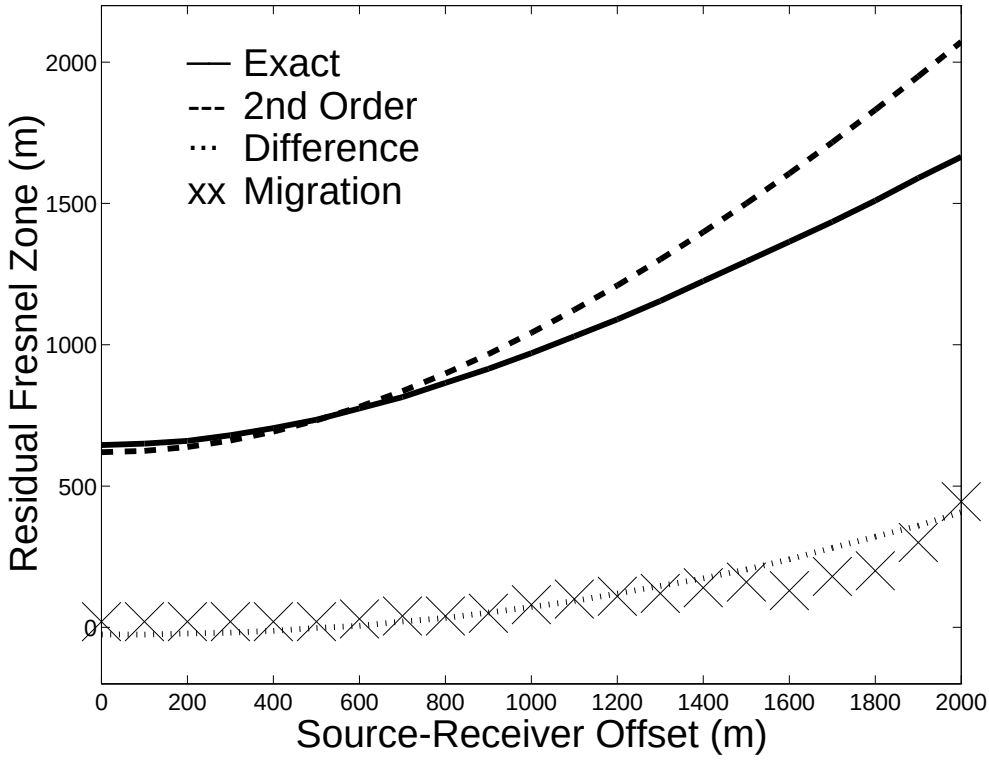

Figure 7: Fresnel zone as a function of offset. Shown are the exact (solid line) and paraxial (dashed line) sizes of the Fresnel zone, their difference (dotted line) and the estimated resolution region (crosses) after Kirchhoff depth migration.

is reached only with perfect, that is, noise-free, correctly sampled, unbiased, data. Any additional distortion due to the wave propagation in an inhomogeneous reflector overburden, such as transmission losses, focusing and defocusing, caustics, etc., as well as acquisition effects such as irregular source and receiver spacing, source and receiver coupling, uncalibrated traces, etc., will not only affect the recovery of the best possible amplitudes but will also degrade the seismic resolution.

SUMMARY

In this paper, we have discussed horizontal resolution of true-amplitude Kirchhoff depth migration in dependence on the source-receiver offset. We have seen that the region around the reflection point affected by the reflected wavefield after migration is closely related to the difference between the time-domain Fresnel zone and its paraxial approximation. Since this difference increases with offset as the paraxial approximation is getting worse, so does the resolution power of seismic migration. A possible explanation of this behaviour is that Kirchhoff migration is an algorithm that is based

on a second-order approximation. Therefore, it can be expected to be correct only up to second order.

Qualitatively, we observe the expected behaviour of a decreasing horizontal resolving power with increasing offset. However, the quantitative behaviour of horizontal resolution as a function of offset is different from that of vertical resolution. As shown by Tygel et al. (1994), for constant velocity and a horizontal reflector, the vertical resolution decreases proportionally to the cosine of the reflection angle. Horizontal resolving power, however, seems not to be a simple function of that angle. The best fitting curve of the type $\cos^q \alpha$ has an exponent of $q \approx 1.5$. The resulting curve, however, does not fit the observed angle-dependence quite well.

ACKNOWLEDGEMENTS

The research of this paper was supported in part by the National Research Council (CNPq – Brazil), the Sao Paulo State Research Foundation (FAPESP – Brazil), and the sponsors of the WIT Consortium.

REFERENCES

Berkhout, A., 1984, Seismic resolution, a quantitative analysis of resolving power of acoustical echo techniques: Geophysical Press.

Beylkin, G., 1985, Imaging of discontinuities in the inverse scattering problem by inversion of a generalized Radon transform: Journal of Mathematical Physics, **26**, no. 1, 99–108.

Bleistein, N., 1984, Mathematical methods for wave phenomena: Academic Press, New York.

Bleistein, N., 1987, On the imaging of reflectors in the earth: Geophysics, **52**, no. 7, 931–942.

Cohen, J., Hagin, F., and Bleistein, N., 1986, Three-dimensional Born inversion with an arbitrary reference: Geophysics, **51**, no. 8, 1552–1558.

Hubral, P., Schleicher, J., and Tygel, M., 1992, Three-dimensional paraxial ray properties – Part I. Basic relations: Journal of Seismic Exploration, **1**, no. 3, 265–279.

Schleicher, J., Hubral, P., Tygel, M., and Jaya, M., 1997, Minimum apertures and Fresnel zones in migration and demigration: Geophysics, **62**, no. 2, 183–194.

Tygel, M., Schleicher, J., and Hubral, P., 1994, Pulse distortion in depth migration: Geophysics, **59**, no. 10, 1561–1569.

Vermeer, G., 1999, Factors affection spatial resolution: Geophysics, **64**, no. 3, 942–953.